Appl. Phys. A 84, 237–242 (2006)
DOI: 10.1007/s00339-006-3628-7

Applied Physics A
Materials Science & Processing

T. GEPPERT[1,2]
S.L. SCHWEIZER[2]
U. GÖSELE[1]
R.B. WEHRSPOHN[2,✉,*]

Deep trench etching in macroporous silicon

[1] Max-Planck Institute of Microstructure Physics, Weinberg 2, 06120 Halle, Germany
[2] Nanophotonic Materials Group, Department Physik, University of Paderborn, Warburger Str. 100, 33098 Paderborn, Germany

Received: 24 April 2006/Accepted: 2 May 2006
Published online: 2 June 2006 •

ABSTRACT We present a method to create at the same time trenches and ordered macropore arrays during photo-electrochemical etching of n-type silicon. This novel method allows in situ separation of single devices with a submicrometer precision. It also enables new device structures in macroporous silicon in the areas of photonics, sensing and electronics. The limits of this new process are simulated using electrostatic models and are verified experimentally.

PACS 82.45.Yz; 81.16.-c

1 Introduction

Since the discovery of macroporous silicon in 1990 [1] and ordered macropore arrays in 1993 [2], numerous applications of this material system have emerged. Hexagonally arranged macropores were the first model system for two-dimensional photonic crystals. Lithographically defined waveguides and microresonators have been realized [3] and first applications such as a miniaturized gas absorption element have emerged [4]. Recently, even three-dimensional photonic crystals have been obtained by modulation of the pore diameter with depth [5]. Other applications are in the area of nanobiotechnology such as biochips or filters [6]. In the area of microelectronics, these structures can be used as capacitors due to their high specific surface area, or in the area of fuel cells they can be used as gas-permeable electrodes [7].

However, most of the current applications rely on pore formation only. Here, we present a method to create at the same time trenches and ordered macropore arrays. This novel method also allows easy separation of single devices with a submicrometer precision. This method is superior to the method described by Ottow et al. [8], since it does not need second lithography and plasma etching steps after photo-electrochemical etching. A few applications of this novel method are described such as coupling layers for photonic crystal devices or as feedthroughs for thermal emitters inside photonic crystals as well as precise alignment markers.

2 Macroporous silicon growth model

The etching method used in this work to produce trenches and ordered arrays of macropores in Si is based on photo-electrochemical etching (PECE) of silicon. This process is revisited briefly below following the model for macropore formation by Lehmann [1, 2]. More comprehensive reviews of different pore regimes and pore-formation mechanisms and alternative models in p-type and n-type Si can be found in [9–12].

While Si is easily etched in aqueous alkaline solutions, it is quite stable in most aqueous acids. However, hydrofluoric acid (HF) is an exception to this general observation. Figure 1a shows the current density j across the HF/n-Si interface vs. the applied voltage V for different illumination conditions. In the regime of cathodic currents (I in Fig. 1a) the Schottky-like HF/n-Si con-

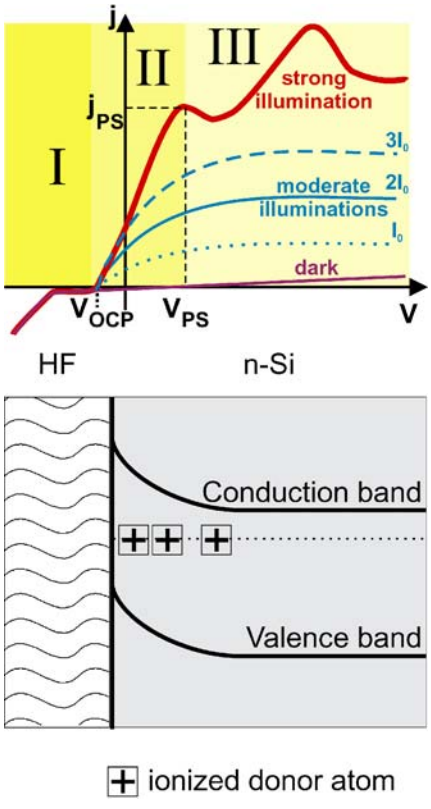

FIGURE 1 (**a**) Schematic plot of current density across the HF/Si interface for n-Si under no (*dark grey*), medium (*light grey*) and strong (*medium grey*) illumination; (**b**) unbiased HF/n-Si Schottky-like contact

✉ Fax: +49 5251 603247, E-mail: wehrspohn@physik.upb.de
*Financial support from the BMBF within the project PHOKISS and the DFG within SPP 1113 is gratefully acknowledged.

tact is forward biased. The current is determined by the majority charge carriers, i.e. the electrons – independent of the illumination state – and leads to the reduction of the H^+ ions in the acidic solution followed by formation of molecular hydrogen (H_2).

The regime of anodic currents (II and III in Fig. 1a) is the more interesting one. Figure 1b shows the arrangement of the valence and conduction bands within n-Si in contact with HF. When the semiconductor Si is brought into contact with the electrolyte HF, the situation resembles a Schottky contact in which the rather conductive electrolyte represents the metal. The different chemical potentials of the aqueous HF and the Si will adapt. This leads to the formation of a Helmholtz double layer in the electrolyte and a surface charge resulting from the ionized donor atoms in the Si, from which a depletion of majority charge carriers (electrons in n-Si) at the HF/Si interface follows. Due to the mobile ions in the electrolyte, the width of the Helmholtz double layer is only a few nm while due to the stationary nature of the donors in Si the depletion region in n-Si is on the order of a few μm wide.

If no illumination is applied to the n-Si, a small (anodic) dark current resulting from thermally generated holes is observed (dark grey line in Fig. 1a).

If the Si is strongly illuminated, the HF/n-Si contact behaves like an HF/p-Si contact (medium grey line in Fig. 1a). An increase in applied voltage V leads to an increase in current across the HF/Si interface. For anodic currents below the critical current density j_{PS} and $V < V_{PS}$ (II in Fig. 1a) divalent[1] dissolution of Si occurs along with the formation of hydrogen. Here the etching current is limited by charge-carrier supply from the Si electrode and porous Si is formed. A suggested reaction is

$$\mathrm{Si} + 4\mathrm{HF}_2^- + \mathrm{h}^+ \rightarrow \mathrm{SiF}_6^{2-} + 2\mathrm{HF} + \mathrm{H}_2 + \mathrm{e}^- , \quad (1)$$

with e^- and h^+ denoting an electron and a hole in the Si [10]. In aqueous HF electrolytes the critical current density j_{PS} was experimentally found to depend only on electrolyte concentration c_{HF} (in weight %) and electrolyte temperature T_{HF} and can be described by

$$j_{PS} = C c_{HF}^{3/2} \mathrm{e}^{-E_a/(k_B T_{HF})} , \quad (2)$$

with C being a constant of 3300 A/cm^2, $E_a = 0.345$ eV and k_B being Boltzmann's constant [2]. For anodic currents and $V > V_{PS}$ (III in Fig. 1a) tetravalent dissolution of Si is observed. In a first step, under consumption of 4 holes, an anodic oxide is formed on the Si electrode:

$$\mathrm{Si} + 2\mathrm{H_2O} + 4\mathrm{h}^+ \rightarrow \mathrm{SiO_2} + 4\mathrm{H}^+ . \quad (3)$$

In a second step this oxide is then chemically etched by the fluorine species HF, $(HF)_2$ or HF_2^- in the electrolyte [10]:

$$\mathrm{SiO_2} + 2\mathrm{HF_2^-} + 2\mathrm{HF} \rightarrow \mathrm{SiF_6^{2-}} + 2\mathrm{H_2O} . \quad (4)$$

Here the current is limited by the chemical reaction rate during the removal of the SiO_2. As a consequence, the Si electrode is electropolished, i.e. all Si surface atoms are removed uniformly.

For medium illumination intensities the IV curve of the HF/n-Si is similar to the light grey curves in Fig. 1a. Here the current density j across the interface is below j_{PS}. j is limited by charge supply from the Si electrode and therefore porous Si is formed.

The electronic holes necessary for the dissolution of Si at the HF/Si interface are created by illuminating the sample with light energy $E_\nu = h\nu \geq E_{g,\,Si} = 1.1$ eV. Due to the high absorption of Si for the IR light used ($\lambda \approx 880$ nm, $\alpha \approx 10^2$ cm^{-1} [10]), electron–hole pairs are produced within the first few μm from the air/Si interface.

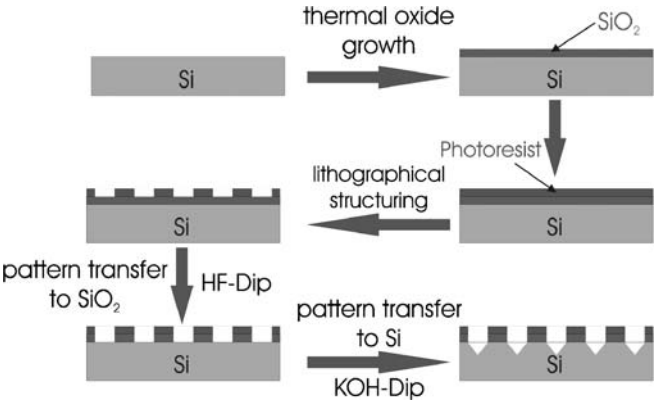

FIGURE 2 Process steps for lithographical prestructuring of a Si wafer for subsequent photo-electrochemical etching

For the formation of porous Si, it is necessary that the current density across the HF/Si interface is smaller than j_{PS}. According to the diameter d_{pore} of the pores, three regimes are distinguished: microporous Si with $0\,\mathrm{nm} \leq d_{pore} \leq 2\,\mathrm{nm}$, mesoporous Si with $2\,\mathrm{nm} < d_{pore} \leq 50\,\mathrm{nm}$ and macroporous Si with $50\,\mathrm{nm} < d_{pore}$. For p-Si $j < j_{PS}$ can only be fulfilled for potentials $V_{OCP} < V < V_{PS}$. For the n-Si used in this work $j < j_{PS}$ can be achieved for potentials $V_{OCP} < V$ by appropriate adjustment of the illumination. Stable macropore growth is possible for $j < j_{PS}$ and $V_{PS} < V$. The ratio j/j_{PS} only controls the average porosity p of the sample. The x–y positions as well as the diameters of individual pores show a random distribution under the constraint of the average porosity being $p = j/j_{PS}$. For ordered arrays of pores in the hexagonal or square lattice, a periodic pattern on top of the Si wafer is defined lithographically and subsequently transferred into the Si as shown in Fig. 2.

By this procedure, so-called 'etch-pits' in the form of inverse pyramids are generated which serve as starting points for the subsequent pore growth. The porosity of such an ordered macropore array is given by

$$p = \frac{j}{j_{PS}} = \frac{A_{Pores}}{A_{Sample}} , \quad (5)$$

with A_{Pores} being the total pore area and A_{Sample} the total HF/Si interface area.

Figure 3 schematically shows the principle of photo-electrochemically

[1] Divalent (tetravalent) means that in the external electrical circuit 2 (4) electrons are necessary for the removal of one Si atom from the electrode.

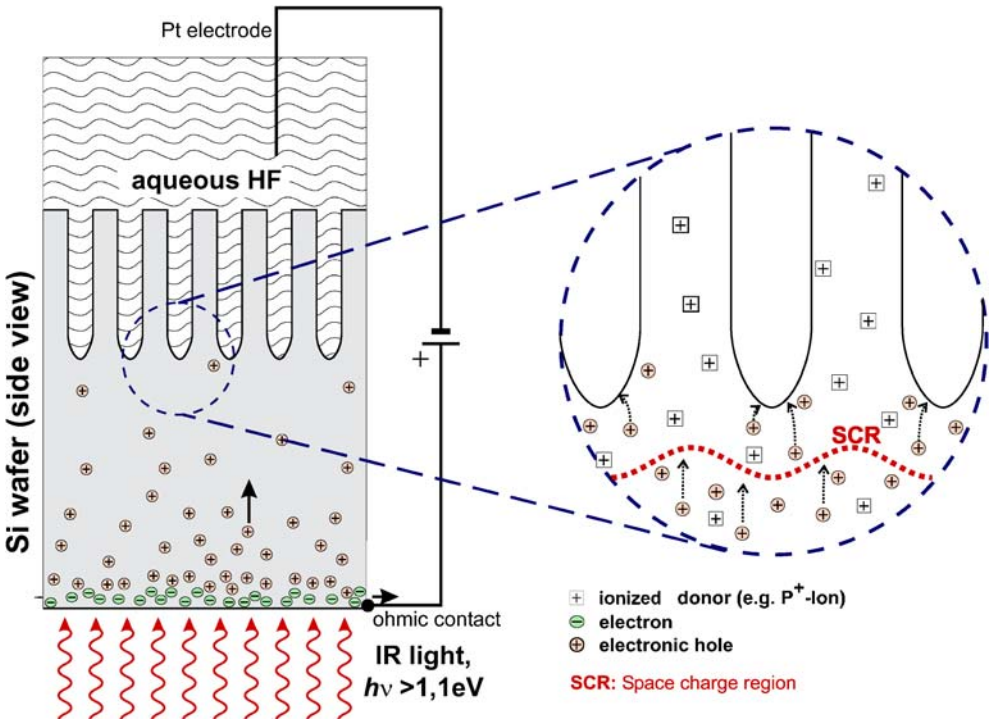

FIGURE 3 Schematic diagram explaining the formation of ordered macropores by photo-electrochemical etching of n-Si under back-side illumination using an anodic potential

etching ordered macropore arrays. Electron–hole pairs are generated by appropriate illumination of the back side of the n-Si wafer. Due to the anodic potential the electrons are sucked away into the voltage source while the holes diffuse through the wafer towards the HF/Si interface where a space-charge region (SCR) has formed. To ensure that the holes can reach the HF/Si interface, high-quality float-zone Si has to be used in which the diffusion length of the holes is on the order of the thickness of the Si wafer. The shape of the SCR follows the physical shape at the interface and is therefore curved. Because the electric field lines are perpendicular to the HF/Si interface, the electronic holes that come into the vicinity of the pore tips are focused onto the pore tips where they promote the dissolution of Si. The width x_{SCR} of the SCR depends on the applied anodic voltage and can be described by

$$x_{\mathrm{SCR}} = \sqrt{\frac{2\varepsilon_0 \varepsilon_{\mathrm{Si}} V_{\mathrm{eff}}}{q N_{\mathrm{D}}}}, \qquad (6)$$

where ε_0 is the free-space permittivity, $\varepsilon_{\mathrm{Si}}$ is the dielectric constant of Si, N_{D} is the doping density of Si and $V_{\mathrm{eff}} = V_{\mathrm{bi}} - V - k_{\mathrm{B}}T/e$ is the effective potential difference between the electrolyte and the Si anode. $V_{\mathrm{bi}} \approx 0.5\,\mathrm{V}$ represents the built-in potential of the contact and V the applied external potential ($k_{\mathrm{B}}T \approx 25$ meV at room temperature). The applied anodic bias has to be chosen high enough such that all of the incoming electronic holes are focused onto the pore tips and none of them penetrate into the Si wall remaining between two pores. If this condition

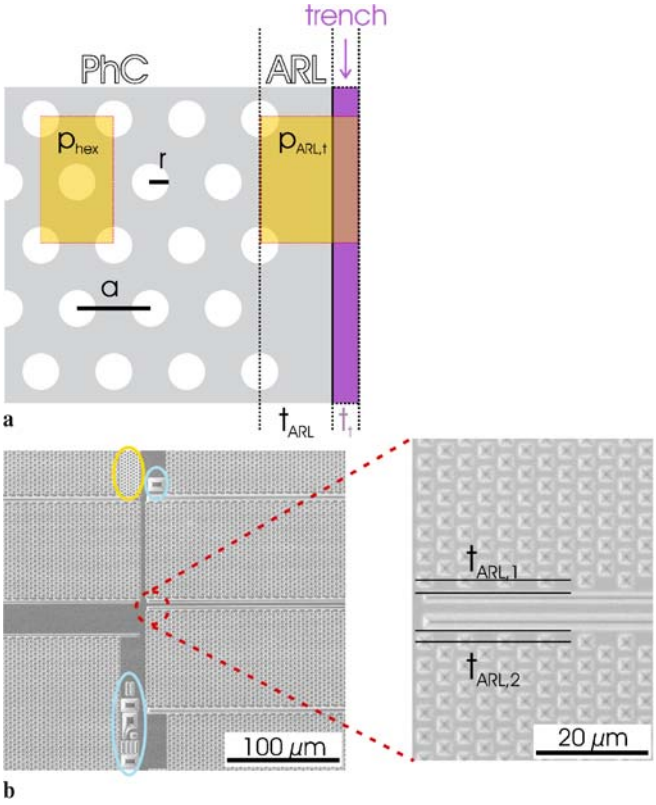

FIGURE 4 Realization of the ARL during PECE. (**a**) Design principle; (**b**) SEM micrographs of the etch pits for the macropores and the trenches in a Si wafer. *Left*: overview; *right*: zoom revealing ARLs with different thicknesses

is fulfilled the pore walls are passivated against dissolution.

The porosity of such an ordered array of macropores with radius r_{Pore}, e.g. arranged in a hexagonal lattice with lattice constant a, can be expressed as

$$p_{\mathrm{hex}} = \frac{2\pi}{\sqrt{3}} \left(\frac{r_{\mathrm{Pore}}}{a}\right)^2 . \tag{7}$$

The growth speed of the pores along the [100] direction in the model of Lehmann depends only on the temperature T_{HF} and the concentration c_{HF} of the electrolyte and can be described by

$$v_{\mathrm{P100}} = \frac{j_{\mathrm{PS}}}{n_{\mathrm{Val}} q N_{\mathrm{Si}}} , \tag{8}$$

with N_{Si} being the particle density of Si ($5 \times 10^{22}\,\mathrm{cm}^{-3}$), $n_{\mathrm{Val}} \approx 2.6$ the dissolution valence for the dissolution process, i.e. the number of electrons supplied by the external circuit needed for the dissolution of one Si atom and $q = 1.6 \times 10^{-19}\,\mathrm{C}$ the elementary charge [2].

3 Extension of the pore-formation model to trench formation

For the realization of the trenches during PECE, it was necessary to go a step further. A trench has to be etched in close proximity to an ordered array of macropores to prevent the formation of non-lithographically defined pores. Keeping in mind the design rule of constant porosity within a unit cell, the thin silicon layer between the last row of pores and the trench, called in the following the ARL, can be realized by lithographically defining a trench to be etched next to the last row of pores (Fig. 4a). The thickness t_{ARL} of the remaining ARL is given by the distance from the edge of the trench to the center of the adjacent pores as shown in Fig. 4b. By lithography the x–y positions of the pores and the trench are fixed. But, the width of the etched trench depends on the r/a ratio chosen during PECE according to

$$t_{\mathrm{trench}} = \frac{\pi \left(\frac{r}{a}\right)^2 (2t_{\mathrm{ARL}} - 0.5)}{\sqrt{3} - 2\pi \left(\frac{r}{a}\right)^2} , \tag{9}$$

with the symbols used in Fig. 4a. As a consequence, the intended r/a ratio has to be taken into account when defining the position of the trench on the lithography mask.

4 Fabrication of trenches and more complex geometries

Because the above arguments concerning porosity are based on simple geometric considerations and the assumption of a homogeneous distribution of charge carriers, it is not expected that the desired ARL thickness is precisely achieved after PECE. For this purpose we performed a series of experiments with different ARL thicknesses around the desired t_{ARL} implemented on the lithography mask.

Figure 5 depicts successfully etched, 450-µm-deep trenches next to arrays of hexagonally arranged macropores. Both the macropores as well as the trenches grow stably. Due to the observance of the before-stated design rules, stable trench-next-to-macropores growth could be achieved by using PECE parameters comparable to the parameter set used for the fabrication of pure macropore arrays. However, it is clear that constant porosity in bulk porous silicon and the ARL/trench regions is a necessary but not sufficient prerequisite to achieve stable macropore/trench growth. If the system is disturbed too much by, for example, creating too thick ARLs with $t_{\mathrm{ARL}} \gtrapprox 1.0a$ the PECE process becomes unstable. As a result, dying out of trenches or branching of pores and trenches is observed as shown in Fig. 6.

However, an increase in roughness of the ARL surface is observed from the scanning electron microscope (SEM) micrographs with increasing depth (Fig. 7). This increase is more pronounced for the thicker ARLs. Atomic force microscope (AFM) micrographs were taken to allow a quantification of this observation. The average surface roughness (root mean square) r_{s} for the device with $t_{\mathrm{ARL}} = 0.6a$ is rather smooth with a value of $r_{\mathrm{s}} = 100\,\mathrm{nm}$. However, with increasing growth depth, r_{s} increases reaching a value of $r_{\mathrm{s}} = 165\,\mathrm{nm}$ in about 350-µm depth.

5 Discussion

The parameters for trench etching are well predicted by (9). How-

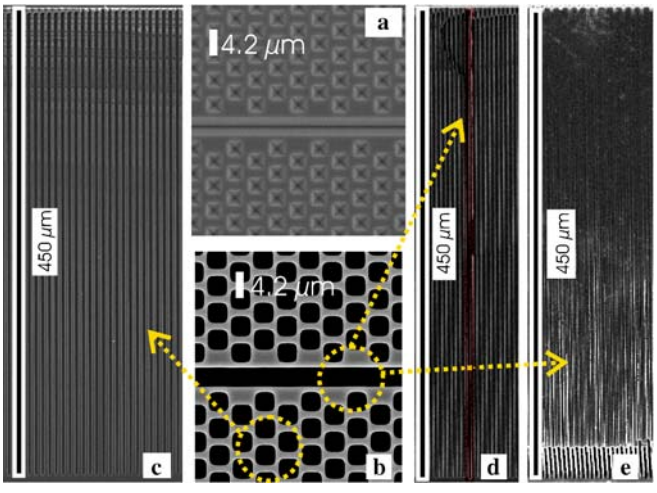

FIGURE 5 Deep trenches next to macropores realized by PECE (SEM micrographs). (**a**) Lithographically prestructured n-Si wafer (top view); (**b**) trench and adjacent macropore array after PECE; (**c**) side view of the cleaving edge through the macropore array; (**d**) side view of the cleaving edge perpendicular to the trench; (**e**) side view of the cleaving edge parallel to the trench (the broken trench surface at the *bottom* is a consequence of cleaving)

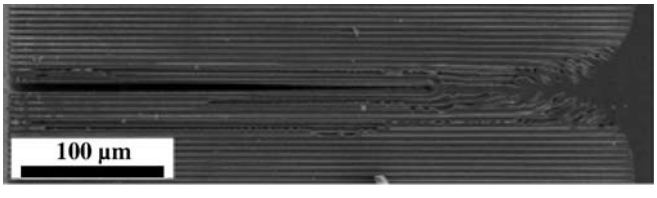

FIGURE 6 SEM micrograph of a trench etched next to a macropore array. The nominal thickness of the ARL is $t_{\mathrm{ARL}} = 1.0a$, resulting in unstable PECE conditions which in turn lead to branching and dying out of pores and trenches

ever, there are limits as evidenced in Fig. 6. A closer look at the SEM micrographs of the device with $t_{ARL} = 1.0a$ reveals the emergence of small holes with diameters on the order of 500 nm after a growth depth of about 30 μm. As these holes do not show up in the device with $t_{ARL} = 0.6a$, it can be concluded that a transition between stable and unstable growth of PECE trenches next to macropores occurs if the ARL is chosen too thick. Both effects, the increase in r_s with growth depth and the instability of the PECE process for thick ARL layers, can be understood by looking at Fig. 8 where the equipotential surfaces for the PhC/ARL geometries used are schematically shown. When homogeneously distributed electronic holes created by illumination at the back side of the Si wafer approach the growth front, they are focussed onto the pore tips and the bottom of the trench, respectively, by the gradient of the potential. In the case of the thick ARL with $t_{ARL} = 1.0a$, a region with only a small potential gradient exists. Here only weak focussing of holes onto either the pore tips or the trench is achieved, resulting in an unstable PECE process. The increase in surface roughness of the ARL is a consequence of the disturbed potential distribution. At the beginning of pore growth the pore and trench locations are determined by lithography. But, the asymmetric potential leads to an inhomogeneous consumption of electronic holes. As a consequence, pore/trench shapes and positions gradually change with increasing depth. In regions where the pores are close to the ARL, the latter will be a little thicker than designed, while, in regions where the pores are further away from the ARL, the ARL can consume more electronic holes during growth and therefore will become slightly thinner than intended. That the pores next to the ARL influence the ARL's surface morphology is also confirmed by the observation that the lateral distance of the vertical stripes on the surface of the ARL is on the order of $\sqrt{3}a$, i.e. the lattice constant along the ΓM direction. This tendency to form a wavy, not perfectly flat surface with vertical texture was observed for all implemented ARL thicknesses $0.5a \leq t_{ARL} \leq 1.1a$, being more pronounced for thicker ARLs. Also, changes in PECE parameters such as temperature 5 °C ≤ $T_{HF} \leq 12$ °C, electrolyte concentration $5\% \leq c_{HF} \leq 7\%$, applied external voltage $1.5\,V \leq V \leq 3.5\,V$, voltage ramps as well as anionic and non-ionic surfactants added to the HF electrolyte did not lead to a suppression of surface roughness. The smaller ripples appearing with a higher spatial frequency might be due to striations, i.e. variations in the doping of the n-Si wafer. These doping inhomogeneities are mirrored in a disturbance of the space-charge region, thereby leading to inhomogeneous pore diameters.

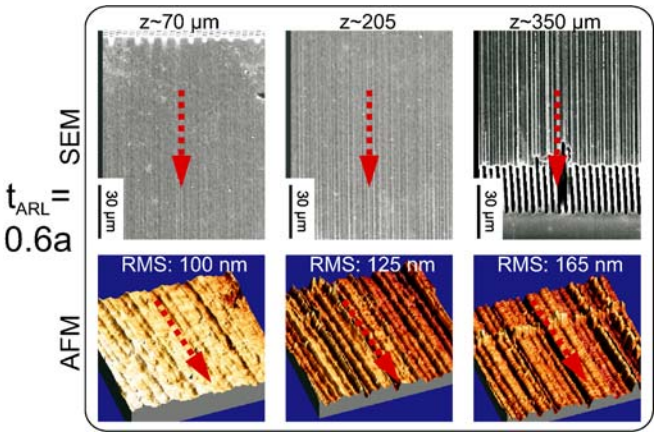

FIGURE 7 SEM and AFM side views of PECE ARLs at different depths after cleaving the sample along the trench. The increase of the roughness of the ARL surface is observed. An image analysis was performed on an area of 35 μm by 35 μm. Parameters: $t_{ARL} = 0.6a$, $r/a = 0.38$, $a = 4.2$ μm, $l_{pore} = 410$ μm

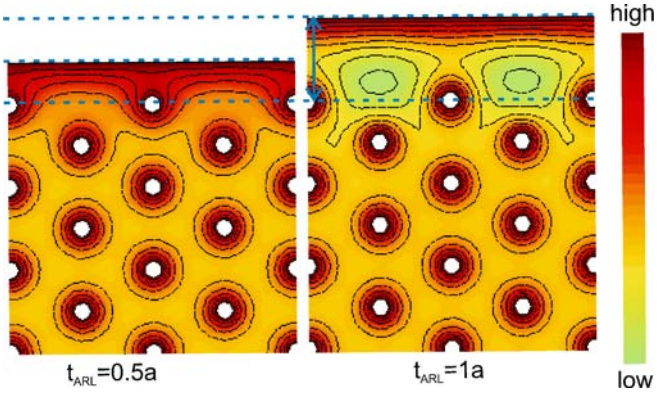

FIGURE 8 Equipotential surfaces for a regular hexagonal pore pattern and at a PhC ARL interface for two different ARL thicknesses during PECE

In the literature, PECE of trenches has been published before by Barillaro et al. [13, 14][2]. However, the trenches etched by Barillaro et al. were parallel to each other, i.e. they etched 'trenches next to trenches' where the symmetry in the vicinity of each trench was the same, namely C_{2v}. In contrast, in the design developed in this work a plane trench faces a corrugated boundary made up by the adjacent air pores. For this reason it can be expected that stable growth of the trenches facing the macropores is harder to achieve. Furthermore, while using comparable lattice constants of about 4–6 μm, the depth of the published trenches is limited to about 30 μm, corresponding to relative low aspect ratios below 10. For comparison, in this work we achieved macropores and trenches with an aspect ratio $\gtrsim 150$.

PECE of trenches, which was originally investigated to enable highly efficient coupling of light to macroporous Si PhC structures [4], allows in addition the realization of novel, interesting structures. Figure 9a and d show how PECE trenches next to macrop-

[2] Christophersen et al. also reported the growth of deep trenches using PECE [15]. But they did not lithographically define trenches to be etched but were investigating Si dissolution and underetching at the edge of a large masked area. Their trenches were only several 10 μm deep and the shape was strongly wedged.

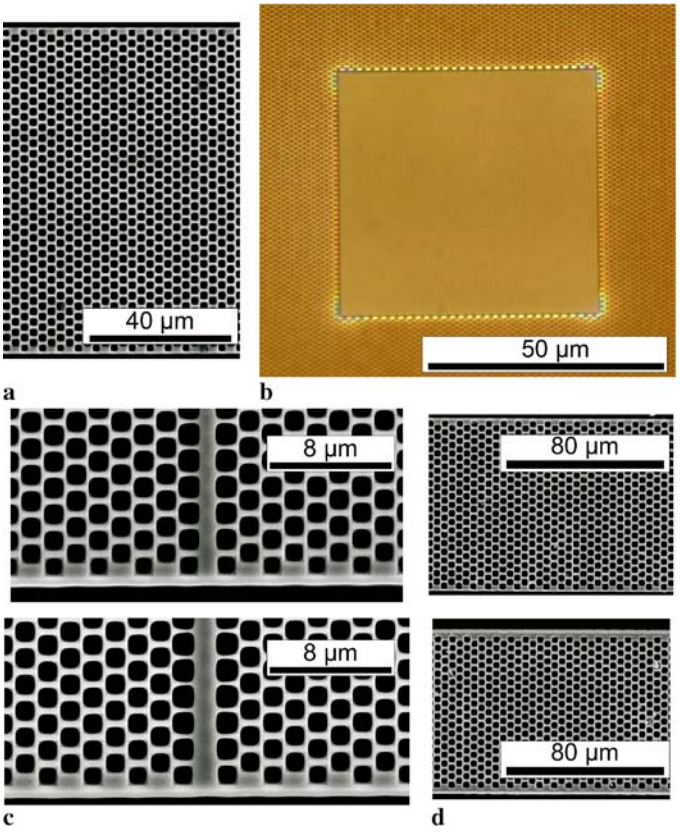

FIGURE 9 PECE trenches: (**a**) two trenches used to define a thin stripe of 61 pore rows in the ΓK direction ($a = 2\,\mu m$); (**b**) trenches along ΓK and ΓM directions to realize a $100 \times 100\,\mu m^2$ hole within a macropore array ($a = 2\,\mu m$); (**c**) W0.7 (*top*) and W1 (*bottom*) PhC waveguides, terminated with an ARL ($a = 2\,\mu m$); (**d**) two trenches used to define thin stripes of 35 (*bottom*) and 39 (*top*) pore rows in the ΓK direction ($a = 4.2\,\mu m$) (SEM: (**a**), (**c**), (**d**); optical microscope: (**b**))

ore arrays can be used to precisely define thin stripes of arbitrary numbers of pore rows along, for example, the ΓK direction. While this is shown for lattice constants of 2 µm and 4.2 µm in Fig. 9a and d, respectively, trench etching is expected to work in principle independent of the lattice constant of the macropore array. These thin stripes are generated during the PECE process without any post processing (except for cleaving using a pair of tweezers). By standard procedures, i.e. inscribing the Si with a diamond scribe and mechanical cleaving, such thin stripes cannot be realized. The thin macropore stripes can e.g. be used to determine the transmission through macroporous Si structures as a function of the sample length. However, effects resulting from the presence of the ARL have to be accounted for. The importance of the surface termination not only of bulk PhCs but also of PhC waveguide structures has been discussed in the literature theoretically [16]. Experimentally, beaming was found to occur at the output side of a W1 waveguide in macroporous Si structures with conventional surface termination [17]. The now available macroporous Si structures with ARL terminations of varying thicknesses allow verification of the theoretically predicted effects (Fig. 9c). Figure 9b shows that PECE of trenches allows realization of well-defined hole structures in macropore arrays. The macropore array in the center of the hole can easily be removed after membrane fabrication by pushing with a small tip or blowing with pressurized air. These holes could be used to host light sources, for mechanically mounting macroporous Si structures onto device substrates or as alignment markers.

6 Conclusion

We presented a method to create at the same time trenches and ordered macropore arrays during photoelectrochemical etching of n-type silicon. Even very deep trenches of more than 400 µm have flat surfaces with an average roughness in the range of 100 nm. The remaining silicon thickness between the trenches and the pore arrays is limited to one inter-pore distance. For larger thicknesses, the trenches do not grow stably. This can be understood by analyzing the equipotential surface during electrochemical etching. This novel method allows in situ separation of single devices with a submicrometer precision. It also enables new device structures in macroporous silicon in the areas of photonics, sensing and electronics.

REFERENCES

1 V. Lehmann, H. Föll, J. Electrochem. Soc. **137**, 653 (1990)
2 V. Lehmann, J. Electrochem. Soc. **140**, 2836 (1993)
3 A. Koenderink, R. Wüest, B. Buchler, S. Richter, P. Strasser, M. Kafesaki, A. Rogach, R. Wehrspohn, C. Soukoulis, D. Erni, F. Robin, H. Jäckel, V. Sandoghdar, Photon. Nanostruct. Fundam. Appl. **3**, 63 (2005)
4 T.M. Geppert, S. Schweizer, J. Schilling, C. Jamois, A. v. Rhein, D. Pergande, R. Glatthaar, P. Hahn, A. Feisst, A. Lambrecht, R. Wehrspohn, Proc. SPIE **5511**, 61 (2004)
5 S. Matthias, F. Müller, C. Jamois, R.B. Wehrspohn, U. Gösele, Adv. Mater. **16**, 2166 (2004)
6 V. Lehmann, Nat. Mater. **1**, 12 (2002)
7 P. French, in *Ordered Porous Nanostructures* (Springer, Heidelberg, 2005), Chap. 7
8 S. Ottow, V. Lehmann, H. Föll, J. Electrochem. Soc. **143**, 385 (1996)
9 P. Allongue, INSPEC data series (1997)
10 V. Lehmann, *Electrochemistry of Silicon* (Wiley-VCH, Weinheim, 2002)
11 H. Föll, M. Christophersen, J. Carstensen, G. Hasse, Mater. Sci. Eng. R **39**, 93 (2002)
12 J. Carstensen, M. Christophersen, G. Hasse, H. Föll, Phys. Status Solidi A **182**, 63 (2000)
13 G. Barillaro, A. Nannini, F. Pieri, J. Electrochem. Soc. **149**, C180 (2002)
14 G. Barillaro, A. Nannini, M. Piottob, Sens. Actuators A **102**, 195 (2002)
15 M. Christophersen, P. Merz, J. Quenzer, J. Carstensen, H. Föll, Sens. Actuators A **88**, 241 (2001)
16 E. Moreno, F. Garcia-Vidal, L. Martin-Moreno, Phys. Rev. B **69**, 121 402 (2004)
17 P. Kramper, M. Agio, C.M. Soukoulis, A. Birner, F. Müller, R.B. Wehrspohn, U. Gösele, V. Sandoghdar, Phys. Rev. Lett. **92**, 113 903 (2004)